

Sierpinski MIMO Antenna for 5G Applications

Abstract. A Sierpinski MIMO antenna was designed in the band of 3.4 – 3.8 GHz for 5G communications is demonstrated in this paper. The proposed antenna is printed on a FR₄ substrate material and dimension of the antenna was 20 × 25 × 0.8 mm³. This paper presents the development of a compact MIMO antenna using a new structure integrated with the Sierpinski using neutralization line and defected ground structure techniques for mutual coupling reduction and antenna isolation improvement. The simulated results proved that the proposed method gives an excellent isolation performance. A good impedance matching return loss of large than 10 dB, high isolation of large than 22 dB at the operating frequency, and low ECC that was 0.026 was simulated across the coveted operating bandwidth.

Streszczenie. W artykule przedstawiono antenę Sierpińskiego MIMO, która została zaprojektowana w paśmie 3,4 - 3,8 GHz dla komunikacji 5G. Proponowana antena jest drukowana na podłożu FR₄, a wymiary anteny to 20 × 25 × 0,8 mm³. W artykule przedstawiono opracowanie kompaktowej anteny MIMO wykorzystującej nową konstrukcję zintegrowaną z anteną Sierpińskiego z wykorzystaniem linii neutralizacji oraz technik uszkodzonej struktury gruntu w celu redukcji wzajemnych sprzężeń i poprawy izolacji anteny. Symulowane wyniki dowiodły, że proponowana metoda zapewnia doskonałą izolację. W pożądanym paśmie roboczym zasymulowano dobre dopasowanie impedancji tłumienia odbicia większe niż 10 dB, wysoką izolację większą niż 22 dB przy częstotliwości roboczej i niskie ECC, które wynosiło 0,02 (**Antena Sierpińskiego MIMO do zastosowań 5G**)

Keywords: MIMO antenna, mutual coupling, Fractal, Isolation, 5G.

Słowa kluczowe: antena MIMO, antena Sierpińskiego, 5G

Introduction

Over 40 years, four generations of wireless mobile phones evolution have been synchronous the technological advancement of hand-held cellular device. At 1990s, elimination of mobile phones antenna was realized, result in revolution of different mobile models with establishing a new wireless service, creation of the cellular advances of the current cycle and advances in technologies of mobile antennas [1].

This revolution triggered increased wireless traffic continuous demands leading to the introduction of the fifth generation (5G) which is the policy makers and wireless engineers interesting pivotal. The 5G wireless network should be supplied by OFDM, Network-LMDS, LAS-CDMA, LAS- CDMA, UWB and IPv6 [2], 4G and 5G are running on last one. Because of such basic protocol depending on location management with assigning IP addresses to mobile nodes, 5G is depending on network access management with it is design that is concerned from worldwide wireless web to mobile devices that lead to waste in resources of such wireless networks, meanwhile it is hard to run IPv6 on which 5G depend [1].

To address such incompatibility problem, a Bandwidth Optimization Control Protocol (BOCP) is proposed and emerge the 5G data path bandwidth [2]. BOCP has implemented between the TCP/IP and MAC layers which roll in bandwidth mix. It is worth to mention, the spectrum of 5G has been classified into two frequency bands of sub-6 GHz and mm- waves. The first one is customizing for the service of citizen radio broadband which is around 3.5 GHz that used the platform structure of 4G Long Term Evolution (LTE) [3], while the second band is above 24 GHz which was approved unanimously by the Federal U.S. Communications Commission (FCC) in June 2016.

In order to pave the way to 5G services of mm waves that comprises of unlicensed and shares spectra. In order to maximize spectrum usage, lots of effort has been directed towards combining and integrating the unlicensed, licensed and shared spectra [4]. However, utilization of microwave frequencies from 3.1 to 10.5 GHz faces challenges related to a number of antennas used which in turn affects the configuration of currently mobile antenna. Meanwhile, spectrum situation of mm-Waves is uncertain and more

complicated [5]. The community of wireless lacking knowledge and experiences of how to dedicate mm radio waves to mobile phones. That exacerbate the situation of strongly entire relation between phone design and major antennas.

Besides, the design of multiple-input multiple-output antennas covering a limited space demands different methods for the increasing of isolation between ports of MIMO antenna, differently, radiation patterns, efficiency, the gain (G), diversity gain(DG) and envelope correlation coefficient (ECC) would be affected [5]. Thus, the mutual coupling reduction techniques should be applied with greater care, and other parameters must be considered. One of the possible solutions to the problem of mutual coupling (MC) is the use of isolation techniques. The isolation decreases between antenna elements and improves the ECC, DG, G and efficiency of the system [1]–[6]. As such, this paper attempted to explain the above-mentioned issues with low MC printed on FR-4 material which covers a centre frequency of 3.6 GHz in the band of 3.4-3.8 GHz.

Antenna Design and Analysis

Fractals theories perform a role in describing the features of complex systems in nature since many things in the real world can be modelled by fractals. So, a fractal is a model that returns itself at smaller scales and results in an irregular shape. The geometrical shape of the rectangular patch with a crossed fractal, as shown in Fig.1. The basic design parameters for the rectangular shape are the dimensional width of 20 mm and the length of 25 mm. The design is achieved using the FR-4 substrate with a thickness of copper (ht = 0.035 mm) and a thickness of FR4 (hs = 0.8 mm). The width of the patch plane is determined using Equation (1)[5]:

$$(1) \quad W_p = \frac{c}{f_r \sqrt{\frac{\epsilon_r + 1}{2}}}$$

The effective constant ϵ_{eff} is calculated by using Equation (2)[5]:

$$(2) \quad \epsilon_{eff} = \frac{\epsilon_r + 1}{2} + \frac{\epsilon_r - 1}{2} + (1 + 12 \frac{h}{w})^{-2}$$

where effective length L_{eff} can be calculated by Equation (3)[5]:

$$(3) \quad L_{eff} = \frac{c}{2f_r \sqrt{\epsilon_{r,eff}}}$$

The fringing length (ΔL) is calculated by Equation (4):

$$(4) \quad \Delta L = 0.412 \frac{(\epsilon_{r,eff} + 0.3) \left(\frac{w}{h} + 0.264 \right)}{(\epsilon_{r,eff} - 0.258) \left(\frac{w}{h} + 0.8 \right)}$$

Length of the patch (L) for proposed microstrip antenna is composed of a rectangular patch, FR-4 substrate, the length of a patch plane is calculate by Equation (5):

$$(5) \quad L = L_{eff} + 2 * \Delta L$$

Calculation of ground plane dimensions is given by Equations (6) and (7):

$$(6) \quad L_g = 6 * ht + L$$

$$(7) \quad W_g = 6 * ht + L$$

In [5], the following empirical formula given in Equation (8) was utilized to calculate the resonant frequency for rectangular patch:

$$(8) \quad f_r = \frac{c}{2L \sqrt{\epsilon_{r,eff}}}$$

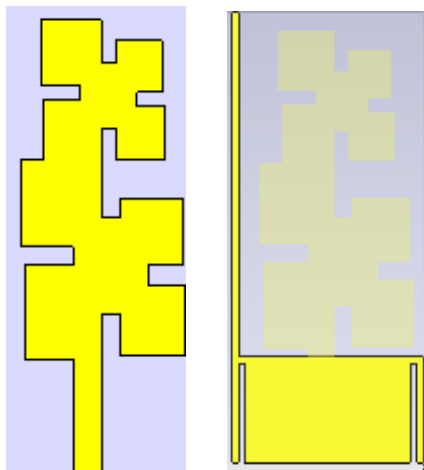


Fig.1: A Fractal Sierpinski single antenna

Fractal sierpinski is one of the several generally used structures in fractal antennas and it is content of equal dimension triangles. This paper used a multiple copy method to build the structure fractal antenna [6], as shown Figure 2.

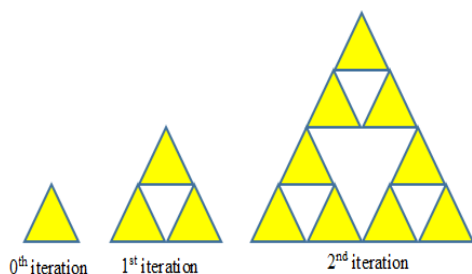


Fig.2: Several Stages of Sierpinski Fractal

During the 1st iteration, the structure was built with three copies of the same shape (triangle) from the 0th iteration, with two triangles at the bottom and the third one on top of these two triangles. 2nd iteration, the same method was returned with the whole structure formed by three triangles in the 1st iteration. Thus, dimensions of the next iteration

raised by a factor of 3 as compared to the dimensions in the previous iteration, which can have been represented by a mathematical formula in Equation (9) [6]:

$$(9) \quad Q \begin{pmatrix} X \\ Y \end{pmatrix} = \begin{pmatrix} r \cos \theta & -s \cos \phi \\ r \sin \theta & s \sin \phi \end{pmatrix} \begin{pmatrix} X \\ Y \end{pmatrix} + \begin{pmatrix} X_0 \\ Y_0 \end{pmatrix}$$

where, r and s are scaling factors, θ and ϕ are rotation angles and X_0 and Y_0 are the values of change. If scaling factors s and r , are reduction or magnification, the change method is self-affine, but if $\theta = \phi$ and $r = s$, the change process is similar. The structure of the MIMO antenna is novel, the initiator is a square patch plane, as shown in Figure 3.a. The length of the arm of the patch square is 8.64 mm ($x = y$). In the next iteration, symmetric four slots cut in the square. The length of the right slot, left slot, down the slot and upper slot are 2.08 mm, 1.6 mm, 32.32 mm respectively with a width of each slot 0.8 mm, as shown in Figure 3.b. The changed square patch is configured by cutting increasable slips to change the dimensions of the arms at the corners in a way to configure asymmetrical corners dimensions, as shown in Figure 3.c.

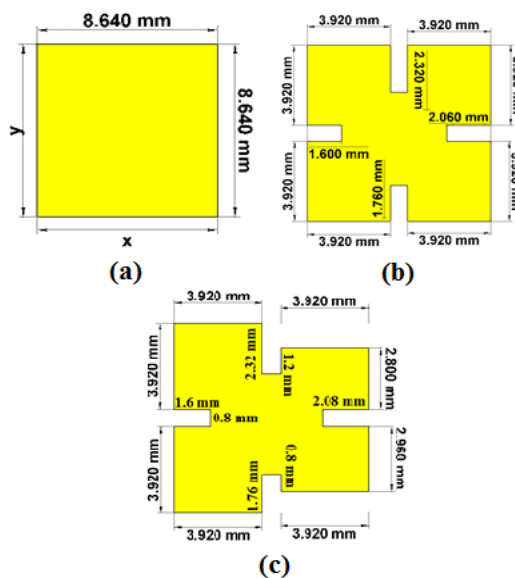


Fig.3: configuration of fractal antenna (a) initiator antenna , (b) 0th iteration (c) modified patch

In Figure 3.c, The upper arm has total length is $3.92x + 1.2y + 0.8x + 2.32y + 3.92x$. The left arm length is $3.92y + 1.6x + 0.8y + 3.92y$. The lower arm length is $3.92x + 0.8y + 0.8x + 0.176y + 3.92x$. The right arm length is $2.8y + 2.08x + 0.8y + 2.96y$. Figure 3. each arm in the square patch has a length of 8.64 mm, but the length of the arms in the changed patch expand. This expedition presents two additional properties in designing the fractal MIMO antenna. The different electrical length of the arms generates many resonant frequencies can be integrated to have wide-operating bands.

The design of proposed fractal printed monopole antenna was started with a square initiator, which consisted of a radiating patch with overall dimensions of 8.64 mm × 8.64 mm, printed a on substrate with dimensions of 20 mm × 25 mm, fixed on the FR4 material with a dielectric constant of 4.3 and a copper lining thickness of $h = 0.8$ mm. The antenna was fed through a microstrip line with a length of 5 mm and a width of 1.2 mm, designed specifically for 50 Ω. On the other side of the substrate, a ground plane was printed with dimensions of 4.7 mm × 8.45 mm. The gap between the square patch and the ground plane was 0.3 mm. The geometry of the reference antenna is shown in

Figure 3.a and the geometry of the square initiator antenna is shown in Figure 3.b. The resonant frequency was calculated by using Equation (10):

$$(10) \quad f_r = \frac{c}{2L\sqrt{\epsilon_r}}$$

The initiator in the new proposed fractal antenna is a square patch, as shown in Figure 3.a. The arms of the patch were equal in dimensions, $x = y = 8.64$, in 0th iteration, as shown in Figure 3.c. In 1st iteration, a mutated square patch, with half of the size of the one used in the previous stage, was added to the shape of fractal antenna, as shown in figure 1. If the x-axis is the bottom of the left modified patch and y-axis passes through the center of the left modified patch in Figure 3.a, Q1 was configured by adding the half sized modified patch to both the left and right sides of MIMO antenna, as shown in Figure 1. The red line mentioned in Figure 4, lies on y-axis and passes through the center (black points) of all the transformation structure Q1. Hence, the scaling factors became $r = s = 0.5$, the rotation angles became $\theta = \phi = 0$ and the transformation factors became $(X_0 = 0, Y_0 = 0.32)$, as shown in Equation (11):

$$(11) \quad Q_1 \begin{pmatrix} X \\ Y \end{pmatrix} = \begin{pmatrix} 0.5 & 0.5 \\ 0 & 0 \end{pmatrix} \begin{pmatrix} X \\ Y \end{pmatrix} + \begin{pmatrix} 0 \\ 0.32 \end{pmatrix}$$

The total length of the upper arm in Figure 3.c was calculated as 12.16 mm, the length of right arm 10.72 mm, the length of left arm 11.84 mm and the length of lower arm 11.2 mm. If the perimeter of the modified square patch is P1 and the perimeter of 1st iteration is P2, can be calculated using Equation (12):

$$(12) \quad P_3 = \frac{1}{2} P_2 = \frac{1}{4} P_1$$

The perimeter of cascade modified patches, Pci at each iteration can be calculated using Equation (13):

$$(13) \quad P_3 = \frac{1}{2} P_{C_{i-1}} \quad i = 1, 2 \text{ and } 3$$

The term (2L) in Equation (10) represents approximately half perimeter of the rectangular patch, so Equation (10) can be rewritten as:

$$(14) \quad f_r = \frac{c}{P\sqrt{\epsilon_r}}$$

However according to [5]:

$$(15) \quad \frac{\text{the perimeter of modified patch}}{\text{the perimeter of square patch}} = \frac{45.92}{34.56} = 1.3287$$

Equation (15) can be written as Equation (16):

$$(16) \quad f_i = \frac{c}{1.3287 P_i \sqrt{\epsilon_r}}$$

Let's suppose, $\frac{c}{\sqrt{\epsilon_r}} = K$, the Equation (17) will be written as Equation (17)

$$(17) \quad f_i = \frac{K}{1.3287 P_i}$$

The proposed MIMO antenna contains two antennas. Each radiating element of the MIMO antenna held a symmetrical monopole antenna fed with a 50 Ω microstrip line. In Figure 4, The proposed MIMO antenna included two separate ports with a distance less than $0.5\lambda = 8.6$ mm, monopoles printed on a 20×25 mm².

For high isolation, neutralization lines were inserted between the two separate antennas of the ground plane and using two defected ground structure to insert two vertical slots in the ground plane. This procedure complemented the two vertical lines of the ground plane, with a width of 0.3 mm and a length of 20 mm to both lines, vertical slots with a width of 0.3 mm and length of 4.4 mm on the ground plane to both slots, as shown in Figure 4.

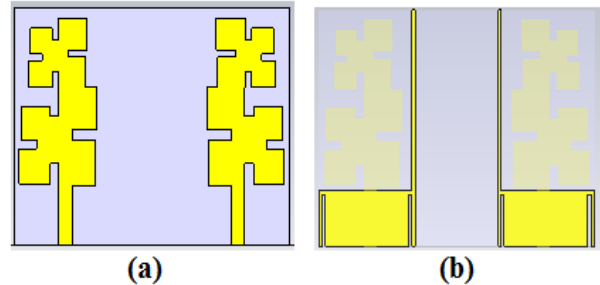


Fig.4: Fractal MIMO antenna (a) Patch plane (b) Ground plane

Performances MIMO antenna

The simulated reflection coefficients (S_{11}) and the fractal antenna isolations (s_{12}) are shown in Figure 5 of design. The fractal antenna has shown a good response within the chosen frequency band. The simulated impedance bandwidth shows good coverage around the resonant frequency of 3.6 GHz. Also, a significant shift in S_{11} is given at a distance of 8.6 mm due to high coupling between the dual-element. In this paper, the main focus is to increase isolation between dual-element MIMO at the wanted band. From these results, the optimum fractal MIMO antenna in this work has been selected at 8.6 mm distance between dual-element due to its overall performance for 5G MIMO application.

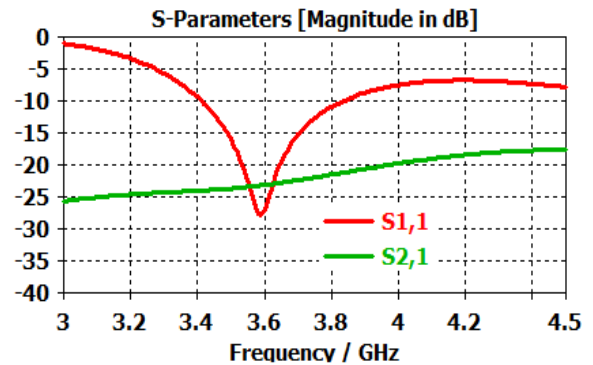


Fig. 5: S-Parameters of the Sierpinski MIMO antenna

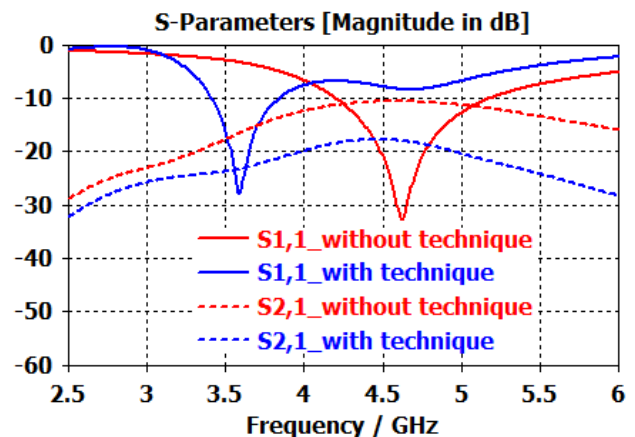


Fig. 6: Isolation (a) without and (b) with isolation techniques

In order to obtain high isolation, NL was inserted between the two separated antenna elements and DGS slots were inserted on the ground plane. The NL used two vertical lines and two slots line on the ground plane. In addition, the parametric study showed that the frequency response and bandwidth of the MIMO antenna are greatly influenced by slots width on the ground plane. An increase or decrease in the width of these slots was found to have induced a change in the centre resonant frequency of the design bandwidth. As can be observed from Fig. 6, the isolation technique significantly increased the isolation between the antenna elements, by a significant reduction in S12 curve. Two Isolation techniques (NL and DGS) were used in the proposed antenna. The hybrid technique reduced the coupling in the ground plane and thereby, increased isolation between the antenna elements. Adding to that, the antennas were placed horizontal, 8.6 mm apart, which further enhances the isolation between the antenna elements.

A maximum envelope correlation coefficients (ECC) obtained was 0.0025 for the band (3.4 - 3.8) GHz for 5G applications, as shown in Fig. 7. In addition, A good level of efficiency 44-55% was obtained from the respective operating band, and the efficiency of the proposed MIMO antenna was above 44% in the operating band.

Diversity gain (DG) is another important factor that must be taken into account while evaluating the performance of MIMO antenna system. It provides information about the reliability of the MIMO system. The higher value of diversity gain signifies better isolation between antenna elements. It depends on the correlation coefficients between antenna signals is given by the following Equation [5]:

$$(18) \quad DG = 10 \sqrt{1 - |ECC|^2}$$

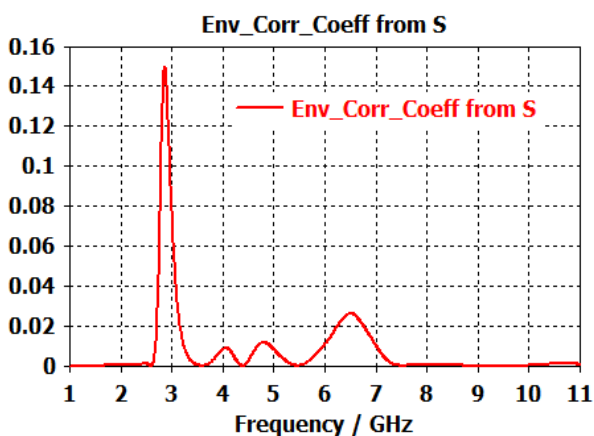


Fig. 7: Simulated ECC of the Sierpinski MIMO Antenna of Band (3.4-3.8) GHz

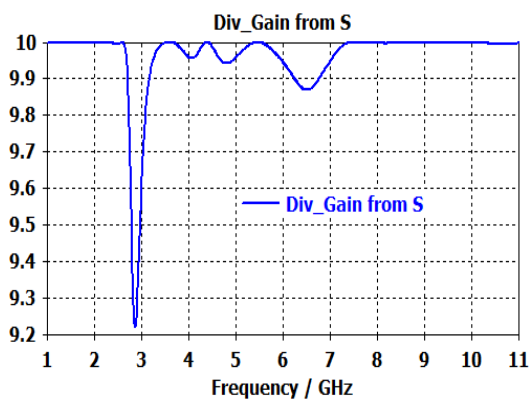


Fig. 8: DG of Disc MIMO Antenna

Figure 8 shows the diversity gain of the proposed design, observed that the suggested MIMO antenna provides high DG > 10.

As shown in Figure 9, the current in the input element was taken at a specific location where the impedance was minimum and the current was maximum, and then its phase was reversed by the hybrid isolation technique. This reverse current was then fed to the nearby antenna to reduce the amount of coupled current. The mutual coupling problem between the two antennas, was solved by NL method. From the surface current distribution in Figure 9, it can be observed that the current is mainly concentrated in around of the slots, which generates inverse surface current and thus, reduces the coupling between the antenna elements.

Fig. 10 shows the simulated radiation pattern of the proposed MIMO antenna for a frequency of 3.6 GHz when Port 1 is excited.

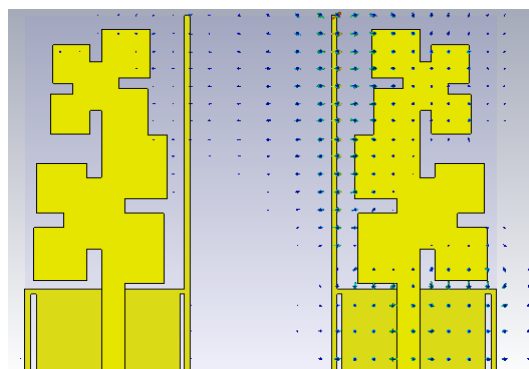


Fig. 9: Simulated current densities with port1 of the fractal Sierpinski MIMO antenna (a) Top view (b) Back view

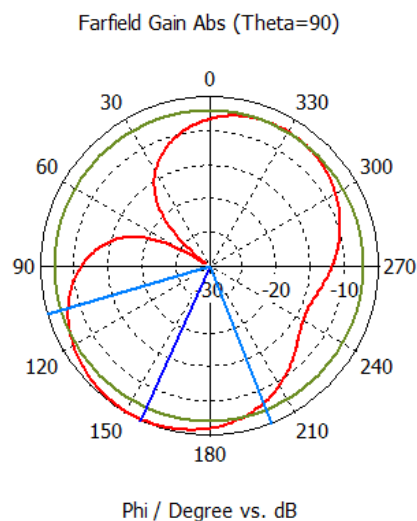


Fig. 10: Radiation Characteristics of proposed antenna at operating frequency 3.6 GHz.

The antenna prototypes were fabricated for the 3.4-3.8 GHz band with an operating frequency of 3.6 GHz, from an inexpensive FR4 dielectric and with overall dimensions of 20 × 25 × 0.8 mm³, as shown in Figure 11. The simulated and measured reflection and transmission coefficients, demonstrated by the two representative antennas, were implied to have a similar level of performance, the antenna prototypes have shown measured isolation 22 dB at operating frequency band. Further, suitable agreement in gain was observed between simulated data and the measured data, as shown in Figure 12.

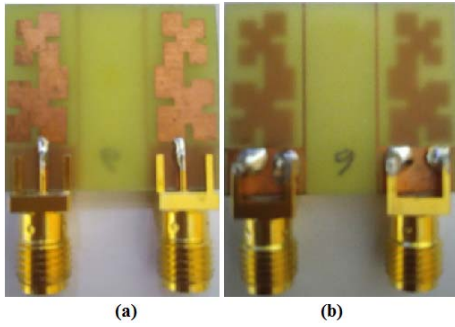


Fig. 11: A photograph of the Fabricated Fractal Sierpinski MIMO Antenna (a) Front View of Band (3.4-3.8) MHz (b) Back View of Band (3.4-3.8)

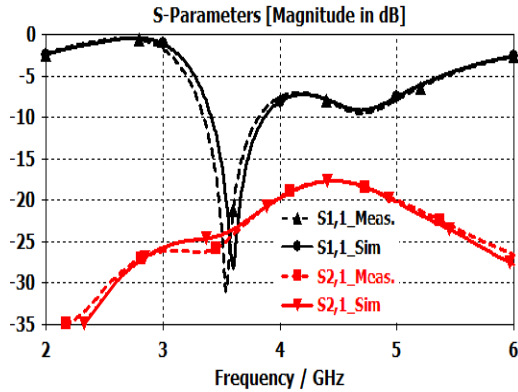


Fig. 12: The Simulated and Measured S-Parameters

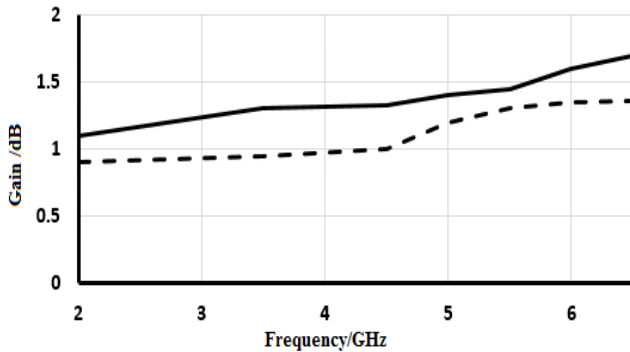


Fig.13: Simulated and Measured Gain of the Fractal MIMO Antenna of Port1

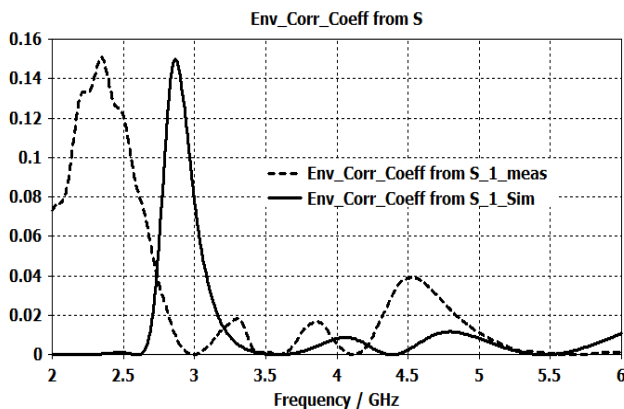


Fig. 14: Simulated and Measured ECC of the Fractal MIMO Antenna

Further, suitable agreement in gain was observed between simulated data and the measured data, as shown in Figure 13. Since the better operation of the MIMO antennas can be got from the incorporation of the ECC in

them, this parameter can be calculated from the S-parameter method by Equation [7] :

$$(19) \quad \rho_{ij}(e) = \frac{|\sum_{n=1}^N S_{ni}^* S_{nj}|}{\sqrt{(1 - \sum_{n=1}^N |S_{ni}|^2)(1 - \sum_{n=1}^N |S_{nj}|^2)}}$$

However, Figure 14 show the results of the proposed MIMO antenna in both simulated and prototypes environment are compatible and confirm the existence of lower ECC between the two adjacent antenna elements.

Validation of the Proposed Antenna

Table 1 shows, the comparison of findings between this research works with other research work. The proposed antenna is compared with several selected types of research. The comparison was based on important characteristics, such as several ports, isolation, efficiency, envelope correlation coefficient, material, bandwidth and size. This V-shaped MIMO antenna is the best for LTE and 5G communications propose for several reasons.

Table 1: Comparisons between the proposed of MIMO antennas and previous related antennas

Ref.	BW (GHz),	Size (mm ²)	Isolation	ECC
[7]	(3.4-3.8)	150 × 200	12.5	< 0.1
[8]	(3.4-3.6)	150 × 75	10	< 0.15
[9]	(3.4-3.8)	60 × 25	15	< 0.02
[10]	(3.2-3.7)	60 × 40	23	<0.002
[11]	(3.6-3.8)	40.5×40.5	17	<0.035
[12]	(3.6-4.2)	31 × 31	10.5	< 0.0024
[13]	(3.6-3.99)	37 × 56	15	< 0.08
[14]	(3.4-3.8)	75×150	15	<0.05
[15]	(4.4-4.9)	21 × 24	18.5	< 0.15
[16]	(3.5-3.6)	40×100	15	<0.03
This work	(3.4-3.8)	20 × 25	22	<0.0026

Conclusion

A mobile phone with a two-element antenna design was proposed for the use of 5G MIMO communications. This job involved the simulation of a novel fractal MIMO antenna for the band range of (3.4-3.8) GHz. The isolation was increased by way of the application of decoupling hybrid technique (neutralization lines and defected ground structure). Besides enhancing the isolation between the antenna elements, the ECC between the signals received by the MIMO antenna ports was sufficiently reduced to meet the specifications for 5G applications.

Acknowledgment

The authors would like to thank Centre for Telecommunication Research and Innovation (CeTRI), Research and Innovation Management (CRIM) and Universiti Teknikal Malaysia Melaka (UTeM) for their encouragement and help for supporting financially to complete this research work.

Authors: Ali Hasan Mousa, Email: alommousa75@gmail.com; Mohd Azlisha bin Othman, Email: azlishah@gmail.com; Mohamed Zoinol Abidin, Email: mohamadzoinol@utem.edu.my; Ayman Mohammed Ibrahim, Email: ayman971972@gmail.com.

REFERENCES

- [1] A. M. Ibrahim, I. M. Ibrahim, and N. A. Shairi, "Review Isolation Techniques of the MIMO Antenna for Sub-6," *Prozrad Elektrotechniczny*, 2021, (01), pp.1-8.
- [2] A. M. Ibrahim, I. M. Ibrahim, and N. A. Shairi, "Compact MIMO Antenna for LTE and 5G Communications," *Prozrad Elektrotechniczny*, 2020, (10), pp.43-46.

- [3] Balanis, C. A., *Antenna Theory Analysis And Design*, 2016, 4th ed., Canada: Wiley.
- [4] A. M. Ibrahim, I. M. Ibrahim, and N. A. Shairi, "Compact MIMO Antenna for LTE and 5G Applications," *Int. J. Microw. Opt. Technol.*, 2020, 15(4), pp.360-368.
- [5] A. M. Ibrahim, I. M. Ibrahim, and N. A. Shairi, "Compact V-Shaped MIMO Antenna for LTE and 5G Applications," *Prozlad Elektrotechniczny*, 2020, (11), pp.84-89.
- [6] Puente, B., C., Romeu, J., Pous, R., and Cardama, A. "On The Behavior of The Sierpinski Multiband Fractal Antenna," *IEEE Transactions on Antennas and Propagation*, 1998, 46(4), pp.517-524.
- [7] A. M. Ibrahim, I. M. Ibrahim, and N. A. Shairi, "Compact MIMO Slots Antenna Design with Different Bands and High Isolation for 5G Smartphone Applications," *Baghdad Science Journal*, 2019, 16, (4), pp.1093-1102.
- [8] Wong, K.-L. and Chang, H.-J., "Hybrid Dual-Antenna for The 3.6-GHz LTE Operation in the Tablet Computer," *Microwave and Optical Technology Letters*, 2015, 57(11), pp.2592-2598.
- [9] Wong, K.-L., Tsai, C.-Y., and Lu, J.-Y., "Two Asymmetrically Mirrored Gap-Coupled Loop Antennas as a Compact Building Block for Eight-Antenna MIMO Array in the Future Smartphone," *IEEE Transactions on Antennas and Propagation*, 2017, 65(4), pp.1765-1778.
- [10] H. S. Singh, Shalini, and M. K. Meshram, "Printed Monopole Diversity Antenna for USB Dongle Applications," *Wirel. Pers. Commun.*, 2016, 86, (2), pp. 771-787.
- [11] K. V. Babu and B. Anuradha, "Design of Multi-Band Minkowski MIMO Antenna to Reduce the Mutual Coupling," *J. King Saud Univ. - Eng. Sci.*, 2018, 6, (3), pp. 51-57.
- [12] I. Suriya and R. Anbazhagan, "Inverted-A based UWB MIMO Antenna with Triple-band Notch and Improved Isolation for WBAN Applications," *Int. J. Electron. Commun. (AEÜ)*, 2019, 99,(5), pp. 25-33.
- [13] A. M. Ibrahim, I. M. Ibrahim, and N. A. Shairi, "Compact Crescent Slot MIMO Antenna with Quad Bands and High Isolation for LTE and 5G communications," *Prozlad Elektrotechniczny*, 2020, (12), pp.19-25.
- [14] S. Chouhan, V. S. Kushwah, D. K. Panda, and S. Singhal, "Spider-shaped fractal MIMO antenna for WLAN/WiMAX/Wi-Fi/Bluetooth/C-band applications," *AEU - Int. J. Electron. Commun.*, 2019, 110, (3) p. 152871.
- [15] N. O. Parchin et al., "Eight-Element Dual-Polarized MIMO Slot Antenna System for 5G Smartphone Applications," *IEEE Access*, 2019, 7,(53), pp. 15612-15622.
- [16] A. M. Ibrahim, I. M. Ibrahim, and N. A. Shairi, "Compact MIMO Antenna for LTE and 5G Applications," *Prozlad Elektrotechniczny*, 2020, (11), pp.84-89.
- [17] C. F. Ding, X. Y. Zhang, S. Member, C. D. Xue, C. Sim, and S. Member, "Novel Pattern-Diversity-Based Decoupling Method and its Application to Multi-Element MIMO Antenna," *IEEE Trans. Antennas Propag.*, 2018. 22, (c), pp. 1-5.